

# Distant Activity of Long-period Comets C/2019 L3 (ATLAS) and C/2020 P3 (ATLAS)

Shaofeng Sun,<sup>1,2</sup> Jianchun Shi,<sup>1,2,3\*</sup> Yuehua Ma<sup>1,2†</sup> and Haibin Zhao<sup>1,2,3</sup>

<sup>1</sup>Key Laboratory of Planetary Sciences, Purple Mountain Observatory, Chinese Academy of Sciences, Nanjing 210023, China

<sup>2</sup>Deep Space Exploration Laboratory / School of Astronomy and Space Science, University of Science and Technology of China, Hefei 230026, China

<sup>3</sup>CAS Center for Excellence in Comparative Planetology, Hefei 230026, China

Accepted XXX. Received YYY; in original form ZZZ

## ABSTRACT

Most Long-period comets remain active at heliocentric distances more than 5 au. Broadband CCD photometry of Long-period comets C/2019 L3 (ATLAS) and C/2020 P3 (ATLAS) are analyzed in this paper. The observation was obtained with three telescopes: ZEISS-1000 at Simeiz Observatory, Maksutov at Abastumani Astrophysical Observatory and ZTSh at Crimean Astrophysical Observatory. For comet C/2019 L3, a fan-shape structure visible in both B and R filters bands can be observed in the northeast direction from the azimuthal averaged images. It possesses a non-steady coma since the average gradient of its surface brightness profile is  $-1.66$ . The R-band  $A(0)f\rho$  values of C/2019 L3 range from  $(5043 \pm 244)$  cm to  $(13\,611 \pm 1874)$  cm, and tend to decrease first and then increase. The average color indices of C/2019 L3 are  $\langle B - V \rangle = 0.75 \pm 0.06$ ,  $\langle V - R \rangle = 0.27 \pm 0.05$ , and  $\langle R - I \rangle = 0.22 \pm 0.05$ . The reddening of C/2019 L3 exhibits variations during the observational runs, from  $(13.75 \pm 1.07) \text{ \%}/\text{k}\text{\AA}$  to  $(-15.69 \pm 0.37) \text{ \%}/\text{k}\text{\AA}$  with an average value of  $(0.94 \pm 0.23) \text{ \%}/\text{k}\text{\AA}$ . While for comet C/2020 P3, an extended coma like a tail can be seen on 2021 May 12. Its R-band  $A(0)f\rho$  values range from  $(606 \pm 31)$  cm to  $(869 \pm 20)$  cm, the color indices are  $B - V = 0.95 \pm 0.07$ ,  $\langle V - R \rangle = 0.29 \pm 0.05$ , and  $R - I = 0.21 \pm 0.05$ , and the reddening is  $(-6.65 \pm 0.01) \text{ \%}/\text{k}\text{\AA}$ . Compared to other Long-period comets, comet C/2019 L3 is very active at heliocentric distance of  $\sim 4$  au, while C/2020 P3 is moderately active at heliocentric distance of  $\sim 7$  au. Besides, the color indices of the two comets differ from those of other Long-period comets.

**Key words:** Long-period comets – photometry – data analysis

## 1 INTRODUCTION

As primitive objects in the Solar System, comets have the same physical and chemical properties as the planetary systems in the early Solar System, which can reveal information about the early Solar System (Mazzotta Epifani et al. 2009; Solontoi et al. 2012). Research on comets can let us further understand the mechanism of planet formation and even solve some basic questions such as the origin of water on Earth (Alexander et al. 2018). Unlike Short-period comets ( $P < 200$  yr), most Long-period comets ( $P > 200$  yr) originate from the Oort Cloud and are entering the inner Solar System for the first time (Jewitt 2015). Long-period comets tend to exhibit stronger activity characteristics than Short-period comets do and appear brighter visually at the same heliocentric distance due to the more volatile components they contain, comparing with the conventional water ice.

Long-period comets also exhibit activity at large heliocentric distances more than 5 au. At this time, the activity is not caused by the sublimation effect of water ice. The current explanation about distant activity of comets mainly includes: the phase transition between amorphous and crystalline water ice (Prialnik 1992; Capria et al. 2002), the annealing of amorphous water ice (Meech et al. 2009),

and the sublimation of more volatile components such as CO<sub>2</sub> (Ootsubo et al. 2012) and/or CO (Jewitt et al. 2019).

There are more than 3000 Long-period comets discovered till 2023 October<sup>1</sup>, while most of them have not been studied in detail. Photometric data in ground-based and space-based surveys allow us to derive physical parameters of Long-period comets, such as absolute magnitude, surface brightness profile of coma, and dust emission rate (Bauer et al. 2022; Betzler et al. 2023). It is generally accepted that Long-period comets originate from the Oort Cloud, and all our knowledge of the Oort Cloud has been yielded by the Long-period comets observed (Fouchard et al. 2023). Furthermore, there remain some significant questions on Long-period comets, such as the evolution of activity, the specific correlations between activity parameters ( $Af\rho$ , slope, etc.), and more detailed group classification (Sárneczky et al. 2016).

In order to enrich the study of Long-period comets, we select two Long-period comets for this work, namely C/2019 L3 and C/2020 P3, which have never been studied before. They are all nearly isotropic comets, both of them having orbital semi-major axis more than 10 000 au. C/2019 L3 and C/2020 P3 reach their perihelion on 2022

\* E-mail: jcsji@pmo.ac.cn (JS)  
† E-mail: yhma@pmo.ac.cn (YM)

<sup>1</sup> Retrieved from MPC, see <https://www.minorplanetcenter.net/mpc/summary> and <https://www.minorplanetcenter.net/iau/lists/PeriodicCodes.html>

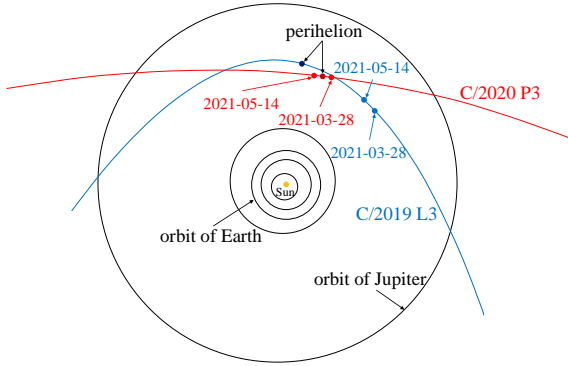


**Figure 1.** Orbit of comets C/2019 L3 and C/2020 P3 in the Solar System. The blue curve is the orbit of C/2019 L3 and the red curve is the orbit of C/2020 P3. Closed curves in black are the orbits of planets in the Solar System. Note that both of these comets have large orbital inclination not shown in this planar graph. The start and end dates of observations as well as the corresponding position of two objects on these dates are marked in this graph.

**Table 1.** Orbital elements of comets C/2019 L3 and C/2020 P3 (Epoch: 2022 July 19).

Comet	e <sup>1</sup>	q <sup>2</sup>	i <sup>3</sup>	Ω <sup>4</sup>	ω <sup>5</sup>	L <sup>6</sup>	B <sup>7</sup>	T <sup>8</sup>
C/2019 L3	1.001 7730	3.554 4290	48.357 10	290.788 50	171.609 70	285.190 94	6.260 14	2459 589.116 50
C/2020 P3	1.000 3270	6.812 3330	61.887 90	19.468 50	82.255 90	93.370 21	60.924 85	2459 325.452 00

<sup>1</sup> eccentricity

<sup>2</sup> perihelion distance

<sup>3</sup> inclination

<sup>4</sup> Longitude of ascending node

<sup>5</sup> Argument of perihelion

<sup>6</sup> Longitude of perihelion

<sup>7</sup> Latitude of perihelion

<sup>8</sup> Time of perihelion passage

January 9 and 2021 April 21, respectively. Fig. 1 shows the planar orbit graph of two comets in the Solar System. Table 1 is the summary on orbital elements of these two comets.

In this paper, we present broadband CCD photometry results of comets C/2019 L3 and C/2020 P3. The circumstance of observations and data reduction process are presented in Section 2. Section 3 describes the photometry results, including morphology, surface brightness,  $Af\rho$  and coma colors. Finally, discussion and conclusions are presented in Section 4.

## 2 OBSERVATIONS AND DATA REDUCTION

### 2.1 Observations

The observations on two comets mentioned above were conducted using three different telescopes belonging to the International Scientific Optical Network (ISON) between 2021 March and 2021 May, namely the 1.0 m Zeiss-1000<sup>2</sup> telescope at Simeiz Observatory (Simeiz), the 2.6 m Shajn Telescope (ZTSh<sup>3</sup>) at Crimean Astrophysical Observatory (CrAO), and the 0.7 m Maksutov meniscus telescope at Abastumani Astrophysical Observatory (AbAO<sup>4</sup>). The technical parameters detailed information of these telescopes are listed in Table 2. Four

<sup>2</sup> <https://link.springer.com/content/pdf/10.1134/S1990341320040112.pdf>

<sup>3</sup> <https://crao.ru/index.php/en/telescopes-en/ztsh-en>

<sup>4</sup> <https://www.oato.inaf.it/blazars/webt/>

<sup>5</sup> [abastumani-astrophysical-observatory-georgia-fsu/](https://github.com/iraf-community/iraf)

**Table 2.** Information of instruments used.

Telescope	CCD Camera	Focal length [mm]	Frame size	Pixel size	Site	MPC Code <sup>1</sup>
ZEISS-1000	FLI	13 000	2048 px × 2048 px 7.3' × 7.3'	0.216 ''/px	Crimea-Simeis	094
ZTSh	FLI PL-4240	10 000	2048 px × 2048 px 14.2' × 14.2'	0.35 μm	Crimea-Nauchnij	095
Maksutov	CCD FLI PL4240	2141	2048 px × 2048 px	13.5 μm	Abastumani	119

<sup>1</sup> see Minor Planet Center Observatory Code at [www.minorplanetcenter.net/iau/lists/ObsCodesF.html](http://www.minorplanetcenter.net/iau/lists/ObsCodesF.html)

**Table 3.** Log of observations on C/2019 L3 and C/2020 P3

Observation Date	r <sup>1</sup> [au]	Δ <sup>2</sup> [au]	Ph.A <sup>3</sup>	Filters <sup>4</sup>	Size[px]	Scale <sup>5</sup> [km/pixel]	Telescope
<b>C/2019 L3</b>							
2021-03-28	4.385	4.916	10.4	B×10, V×10, R×10	1018 × 1018	2075	ZEISS-1000
2021-04-02	4.360	4.933	10.1	B×4, V×4, R×5	2048 × 2048	4654	Maksutov
2021-04-03	4.355	4.936	10.1	B×5, V×5, R×6	2048 × 2048	4658	Maksutov
2021-04-04	4.350	4.939	10.0	B×10, V×10, R×10	2048 × 2048	4660	Maksutov
2021-04-08	4.331	4.950	9.7	B×6, V×5, R×5	2048 × 2048	4670	Maksutov
2021-04-12	4.311	4.960	9.5	B×4, V×5, R×3	2048 × 2048	4684	Maksutov
2021-04-14	4.301	4.965	9.3	B×4, V×5, R×5	2048 × 2048	4686	Maksutov
2021-04-15	4.296	4.967	9.3	B×4, V×4, R×4	2048 × 2048	4687	Maksutov
2021-05-04	4.205	4.987	8.0	B×10, V×10, R×10, I×10	1365 × 1365	1587	ZEISS-1000
2021-05-10	4.177	4.985	7.6	B×3, V×3, R×3, I×3	2048 × 2048	4709	Maksutov
2021-05-12	4.168	4.984	7.5	B×5, V×5, R×5, I×5	2048 × 2048	4706	Maksutov
2021-05-14	4.159	4.982	7.4	B×11, V×11, R×12, I×11	1024 × 1024	2015	ZTSh
				B×7, V×7, R×7, I×7	2048 × 2048	4706	Maksutov
<b>C/2020 P3</b>							
2021-03-28 <sup>7</sup>	6.956	6.814	8.2	B×7, V×7, R×7	1018 × 1018	2937	ZEISS-1000
2021-04-02	6.990	6.813	8.2	V×11, R×14	2048 × 2048	6592	Maksutov
2021-05-11	7.216	6.814	7.6	C×4, V×5, R×5	2048 × 2048	6807	Maksutov
2021-05-12	7.221	6.814	7.6	B×3, V×3, R×3, I×3	1024 × 1024	2914	ZTSh
				B×6, V×5, R×5, I×5	2048 × 2048	6807	Maksutov

<sup>1</sup> heliocentric distance

<sup>2</sup> geocentric distance

<sup>3</sup> phase angle

<sup>4</sup> numbers after ‘×’ indicate amounts of images under corresponding filters, ‘C’ means ‘clear glass’

<sup>5</sup> size of original image

<sup>6</sup> the calculated image scale in km per pixel

<sup>7</sup> images on this date are too faint to use

kinds of broadband observational data were obtained with broadband B, V, R and I filters in the Johnson-Cousins system. Broadband B, V, R and I filters in the Johnson-Cousins system were used to obtain the observational data. The log of all observations is presented in Table 3. Most of the data were obtained from telescope Maksutov. For comet C/2019 L3, the observations were carried out before the time of perihelion, while for comet C/2020 P3, it was near its perihelion during the observation period.

### 2.2 Data reduction

All of the images had been corrected with common methods for dark subtraction, bias subtraction and flat-field normalization when ISON provided the observational data for this research. In order to raise improve the signal-to-noise ratio, images on different observational dates were aligned and sum combined for different filters according to the photocenter of comet. The same thing was also done on the basis of photocenter of background star as the motion of comet in each frame is obvious. Several tasks such as center, imshift and combine in IRAF (the Image Reduction and Analysis Facility)<sup>5</sup>, were applied for this procedure. Since the comet and reference stars for photometry are in the same frame, the airmass correction is not necessary can be neglected. Given that some images are in the case where comet gets too close to the background stars around, psf subtraction was conducted to cover up these stars with tasks such as substarr.

The photometric calibration of these two comets’ data was performed with the UCAC4 (Zacharias et al. 2013) and UCAC5 (Zacharias et al. 2017). Additionally, the GCVS 5.1 (Samus’ et al.

2017) was applied to inspect the variability of all the comparison stars.

In order to measure the instrument magnitudes of comets and comparison stars, circular aperture photometry was applied. When conducting aperture photometry on stars, the sky background value is determined by the annular region around the star. However, when conducting aperture photometry on comets, the sky background value is determined by several clean background areas far away from the comet. The photometric aperture of comparison stars was determined by nearly 2 times the full-wide at half-maximum (FWHM). Since three different telescopes were involved during the observation, the photometry of comets was performed on different apertures centered on the comet photocenter, with all of them ensured to be up to 1.5 times the full-wide at half-maximum and close to each other in arcsecond as much as possible. The ranges of seeings for the three telescopes are as follows: 1.2'' to 7.5'' for ZEISS-1000, 3.9'' to 7.8'' for Maksutov, and 2.4'' to 3.9'' for ZTSh. The photometric results are listed as Table 4, and the error of photometry  $e_{\text{phot}}$  is derived from equation (1) as follows:

$$e_{\text{phot}} = \sqrt{e_c^2 + \sigma_s^2}, \quad (1)$$

where  $e_c$  is the magnitude error of comet from IRAF photometric file and  $\sigma_s$  is the standard deviation of the calibration values in differential photometry.

## 3 RESULTS

### 3.1 Morphology

The original images of C/2019 L3 in the R band exhibit greater clarity compared to images in other bands, and they all resemble a star-like appearance. On the other hand, the original images of C/2020 P3 appear very faint, and the ones taken in the R band are also relatively clearer than those in other bands. Unlike C/2019 L3, some images of C/2020 P3 reveal the presence of an extended tail. After applying the data reduction process mentioned before, we get one image for each filter on each observational date. Fig. 2 is a thumbnail view of the reduction result with comet located in center of each small parts whose field of view are all 2' × 2'. Two different telescopes were involved in observing comet C/2019 L3 on 2021 May 14, thus in Fig. 2 there are two groups of thumbnails on this date with the upper one by telescope ZTSh and the lower one by telescope Maksutov, and the same applies to comet C/2020 P3 on 2021 May 12. The black spots in several part of this view are due to result from the psf subtraction process, as it is not always perfect for star subtraction. For comet C/2019 L3, the observational record is abundant. The I band filter was added in the observation from 2021 May, providing more data for this study. From the combined images of C/2019 L3, it is easily to notice that this comet is very round and seemingly isotropic. For comet C/2020 P3, there are few data and in some cases it is hard to identify in single image the image resolution is lower and it is not easily discernible. However Nevertheless, its extended coma looking like a tail is more obvious, especially for the images taken on 2021 May 12, which roughly measured 20'' from comet center in R-band image.

For morphology analysis, it is necessary to apply some image enhancement techniques with which we can recognize some features and structures hidden in coma (Samarasinha & Larson 2014). Many pieces of software have been developed for comet image enhance-

**Table 4.** Photometric results of comet C/2019 L3 and C/2020 P3.

	$\rho [\text{arcsec}']$	B	V	R	I	$B - V$	$V - R$	$R - I$
<b>C/2019 L3</b>								
2021-03-25.729	14.5	14.32 ± 0.09	13.72 ± 0.07	13.17 ± 0.15	-	0.60 ± 0.11	0.55 ± 0.16	-
2021-04-02.739	15.6	14.37 ± 0.10	13.62 ± 0.04	13.14 ± 0.06	-	0.75 ± 0.11	0.48 ± 0.07	-
2021-04-03.719	15.6	14.25 ± 0.05	13.55 ± 0.03	13.08 ± 0.07	-	0.70 ± 0.05	0.47 ± 0.08	-
2021-04-04.691	15.6	14.26 ± 0.05	13.55 ± 0.02	13.32 ± 0.01	-	0.70 ± 0.05	0.23 ± 0.02	-
2021-04-08.691	15.6	14.33 ± 0.05	13.44 ± 0.02	13.36 ± 0.01	-	0.88 ± 0.05	0.09 ± 0.03	-
2021-04-12.724	19.5	14.22 ± 0.05	13.33 ± 0.01	13.19 ± 0.01	-	0.89 ± 0.05	0.14 ± 0.02	-
2021-04-14.702	15.6	14.21 ± 0.04	13.51 ± 0.03	13.29 ± 0.02	-	0.71 ± 0.05	0.21 ± 0.03	-
2021-04-15.714	15.6	14.23 ± 0.03	13.51 ± 0.01	13.28 ± 0.02	-	0.72 ± 0.04	0.23 ± 0.02	-
2021-05-04.736	11.0	14.32 ± 0.04	13.75 ± 0.04	13.42 ± 0.04	13.25 ± 0.03	0.57 ± 0.05	0.33 ± 0.06	0.17 ± 0.05
2021-05-10.735	15.6	13.96 ± 0.03	13.24 ± 0.01	13.05 ± 0.03	12.80 ± 0.04	0.72 ± 0.04	0.18 ± 0.03	0.26 ± 0.05
2021-05-12.724	15.6	14.14 ± 0.03	13.27 ± 0.03	13.11 ± 0.02	12.90 ± 0.03	0.87 ± 0.05	0.16 ± 0.04	0.22 ± 0.04
2021-05-14.721	14.0	14.21 ± 0.04	13.28 ± 0.04	13.13 ± 0.02	12.90 ± 0.06	0.93 ± 0.06	0.15 ± 0.04	0.24 ± 0.06
<b>C/2020 P3</b>								
2021-04-02.775	13.0	-	17.61 ± 0.05	17.24 ± 0.03	-	-	0.37 ± 0.05	-
2021-05-11.744	13.0	-	18.15 ± 0.05	17.83 ± 0.04	-	-	0.32 ± 0.06	-
2021-05-12.749	6.7	19.00 ± 0.06	18.05 ± 0.03	17.88 ± 0.02	17.67 ± 0.04	0.95 ± 0.07	0.17 ± 0.04	0.21 ± 0.05

<sup>1</sup> UT time at the beginning of exposure

<sup>2</sup> the photometric aperture in arcsecond

ment, such as Astroart<sup>8</sup> and online tool Cometary Coma Image Enhancement Facility<sup>7</sup>. In this work, we applied azimuthal renormalization method on images of C/2019 L3 on 2021 May 14 by telescope Maksutov since other images are too faint and show no evident features after enhanced. The result is shown in Fig. 3, where the enhanced images under V and R filters show a small northeastward fan-shape structure, while the enhanced images under B and I filters give no obvious feature.

### 3.2 Surface brightness profile

Based on the photometric results, the radial surface brightness profile (SBP) was computed as the function of the angular distance  $\rho$  measured from the photocenter of comet. For this purpose, every image was trimmed from the center of the comet, and the sky value was determined by the median of the trimmed image. In the case of a steady-state coma, the surface brightness  $B$  is expected to follow a power-law relation with  $\rho$  as  $B \propto \rho^m$ , where  $-1.5 \leq m \leq -1.0$ , and the index  $m$  is often referred to as the gradient ( $m = d \lg B / d \lg \rho$ ). As the radiation pressure accelerates the dust particles, the value of  $m$  decreases and approaches  $-1.5$  in the limiting case (Jewitt & Meech 1987). Conversely, if the index  $m$  falls below  $-1.5$ , it suggests the presence of nonsteady dust coma emission (Lowry et al. 1999).

Not only in single images does comet C/2019 L3 appear like a stellar, but also in stacked images. However, the SBP of C/2019 L3 shows it clearly the excess flux in outer region compared with stellar SBP. In Fig. 4 we report an example plot of the R-band SBP as a function of  $\lg \rho$  for C/2019 L3 observed on 2021 May 4. The gradient  $m$  in the  $0.5 \leq \lg \rho \leq 1.0$  range is calculated by the least-squares fit to  $\lg B$  versus  $\lg \rho$ . In Fig. 5, the gradients of C/2019 L3 on each date are depicted, and the averaged value is indicated by a blue dotted line. Note that in Fig. 4 the SBP is expressed as magnitude, and according to the relationship between magnitude and luminous intensity, the slope in such figure should be multiplied by  $-0.4$  to make the gradient  $m$ . The averaged  $m$  is  $-1.66$ , and in most cases it is below  $-1.5$ , indicating that this comet's dust emission is in a nonsteady state. While for comet C/2020 P3, all images taken are so faint and it would bring about a great deal of uncertainty if we calculated its SBP.

### 3.3 $A f \rho$

The  $A f \rho$  value introduced by A'Hearn & Schleicher (1984), where  $A$  represents the grain albedo,  $f$  the filling factor, and  $\rho$  the aperture,

<sup>6</sup> [https://www.msb-astroart.com/down\\_en.htm](https://www.msb-astroart.com/down_en.htm)

<sup>7</sup> <https://www.psi.edu/research/cometimen>

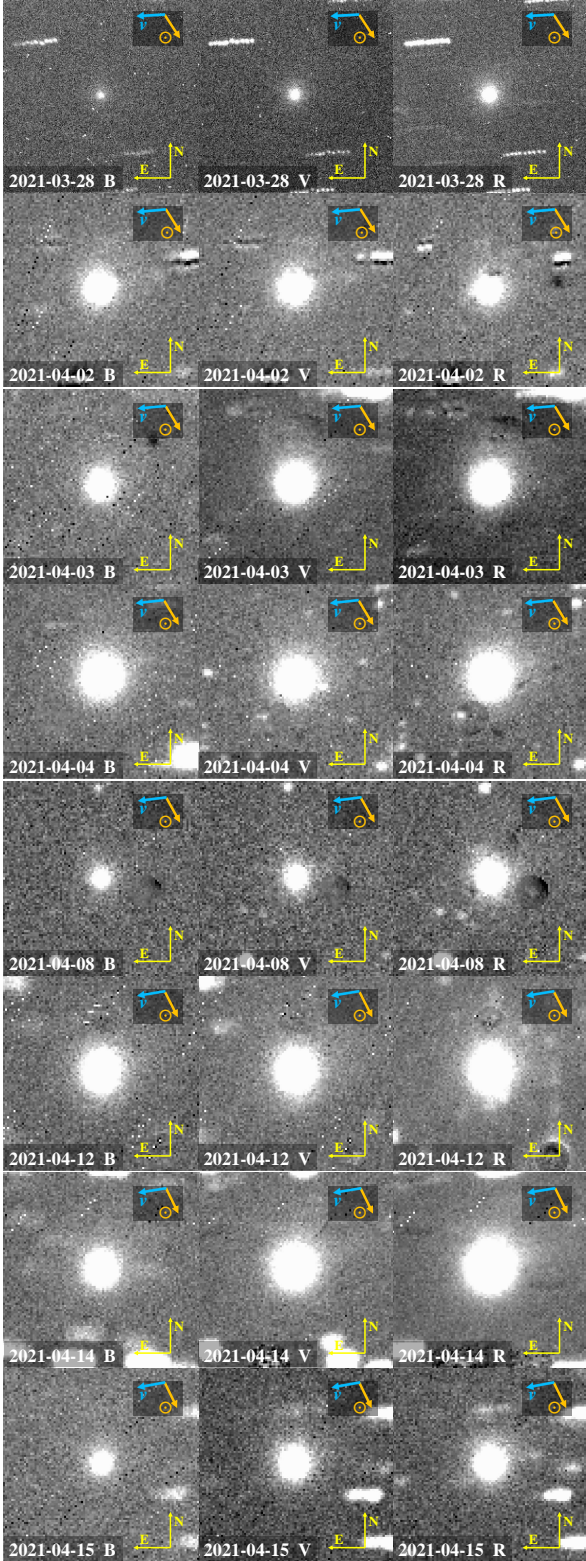


**Figure 2.** The processed images of comet C/2019 L3 and C/2020 P3 in different filters, with north at the top and east to the left. The field of view is  $2' \times 2'$  for each thumbnail. Blue arrow shows the direction of the comets' velocity, and the orange arrow shows the direction to the Sun.

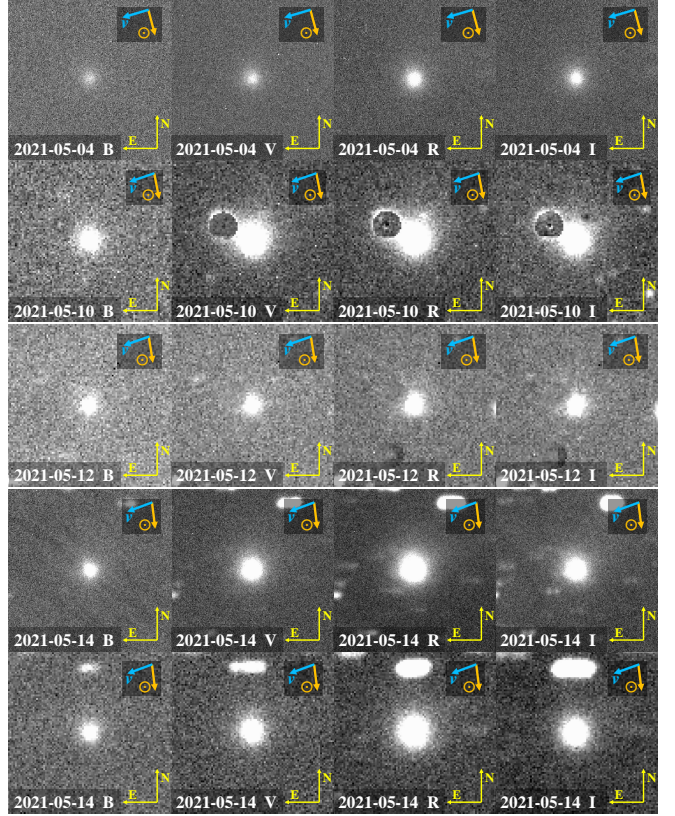


**Figure 2. (Continued)**

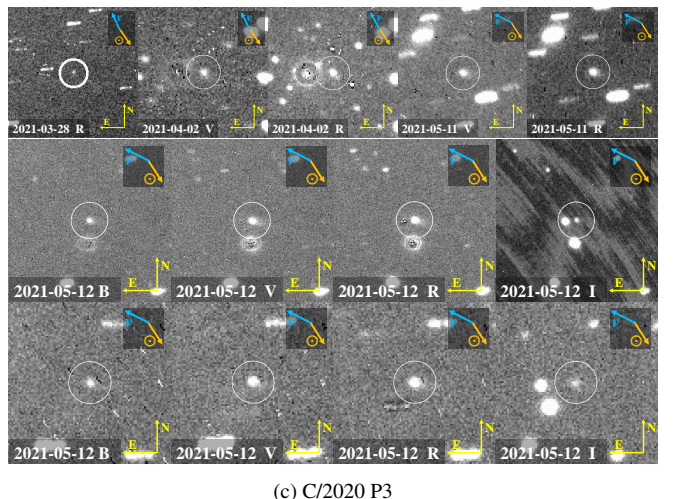


**Figure 2. (Continued)**

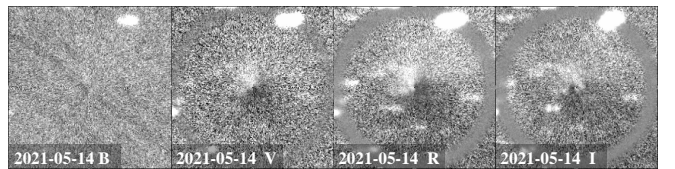


**Figure 3.** Azimuthal renormalized image of C/2019 L3 on 2021 May 14, the field of view for each thumbnail is also  $2' \times 2'$ .

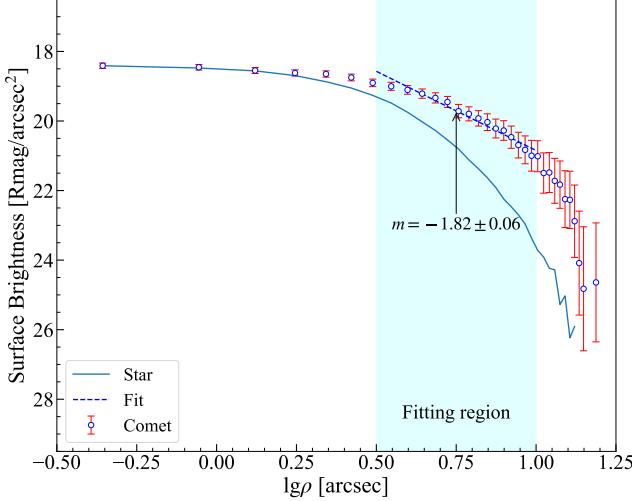


**Figure 4.** An example figure for R-band surface brightness of comet C/2019 L3. The error plot is the SBP of comet, and the blue solid line is the SBP of a background star. The blue dotted line is a linear regression result of comet's SBP vs  $\lg \rho$  with  $\lg \rho$  between 0.5 and 1.0, and the gradient  $m$  related to the slope is marked on the graph with an arrow.

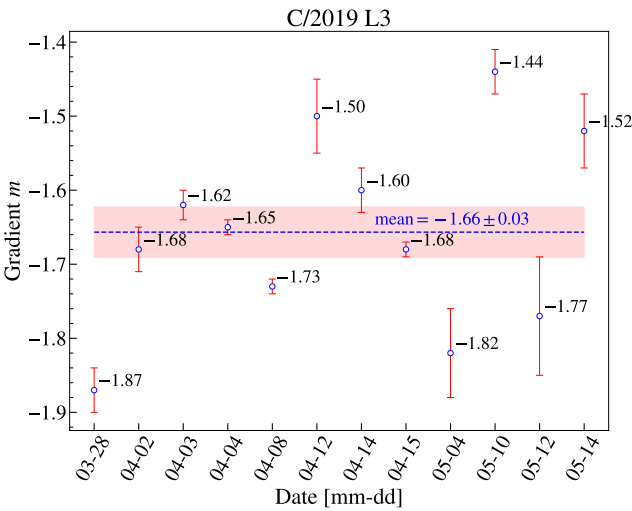


**Figure 5.** The  $m$  of R-band surface brightness of comet C/2019 L3 with date, blue dashed line is the averaged  $m$ , around which is a red shadow representing the error.

is commonly used to indicate the dust production activity of comets. Usually it is expressed in cm as equation (2):

$$Af\rho = \frac{4r^2\Delta^2}{\rho} 10^{0.4(M_\odot - M_c)}, \quad (2)$$

where  $r$  is the heliocentric distance in units of [au],  $\Delta$  the geocentric distance in units of [km],  $\rho$  the aperture in units of [km],  $M_\odot$  the absolute magnitude of the Sun (respectively  $-26.13$  and  $-27.15$  for B and R filters, see Willmer 2018), and  $M_c$  the corresponding magnitude of comet under the aperture of  $\rho$ .

Due to the phase darkening effect, it is necessary to adjust  $Af\rho$  values at different phase angles to a specific angle. In this work, all observations were conducted at small phase angles, and we normalize the  $Af\rho$  values to a phase angle of  $0^\circ$  using equation (3), as shown

**Table 5.**  $Af\rho$  values for comet C/2019 L3 and C/2020 P3.

Observation Time	$Af\rho$ [cm] ( $\rho = 10^4$ km)	$Af\rho_{\max}$ [cm]	$\rho_{\max}$ [km]
<b>C/2019 L3</b>			
2021-03-28.729	$13\,611 \pm 1874$	$13\,615 \pm 1875$	10 373
2021-04-02.739	$9332 \pm 539$	$10\,748 \pm 618$	20 930
2021-04-03.719	$7959 \pm 143$	$10\,869 \pm 729$	22 093
2021-04-04.691	$6220 \pm 69$	$9003 \pm 114$	20 930
2021-04-08.691	$8985 \pm 603$	$8700 \pm 110$	19 860
2021-04-12.724	$7911 \pm 102$	$7410 \pm 269$	29 343
2021-04-14.702	$7320 \pm 95$	$8268 \pm 133$	25 822
2021-04-15.714	$5043 \pm 244$	$8891 \pm 154$	19 953
2021-05-04.736	$5943 \pm 96$	$8320 \pm 340$	29 365
2021-05-10.735	$7523 \pm 134$	$8787 \pm 205$	29 343
2021-05-12.724	$5701 \pm 236$	$9590 \pm 157$	21 127
2021-05-14.721	$6356 \pm 152$	$9164 \pm 95$	29 343
<b>C/2020 P3</b>			
2021-04-02.775	$869 \pm 20$	$948 \pm 19$	15 789
2021-05-11.744	$708 \pm 17$	$848 \pm 17$	19 048
2021-05-12.749	$606 \pm 31$	$801 \pm 38$	19 048

below:

$$A(0)f\rho = \frac{A(\alpha)f\rho}{\phi(\alpha)}, \quad (3)$$

where  $\alpha$  is the phase angle, and  $\phi$  is the phase function. A composite phase function (see Schleicher & Bair 2011; Marcus 2007) suggested by D. Schleicher<sup>8</sup> is suitable for adjustment in this work. The related data ([dustphaseHM\\_table.txt](#))<sup>9</sup> provides the phase function with phase angle in the  $0^\circ \leq \alpha \leq 180^\circ$  range, and we adopt cubic spline interpolation method on it to obtain unlisted values.

Fig. 6 shows some part of the R-band  $Af\rho$  profiles, and results for the maximum of  $Af\rho$  and the aperture corresponding to this maximum are summarised in Table 5. When a comet possesses steady coma, its  $Af\rho$  will be independent of aperture. In this paper, as is shown in Fig. 6, that is not the case for comet C/2019 L3 or C/2020 P3, both of which reveal a steep increase in  $Af\rho$  with the aperture  $\rho$  near the comet center along with a smooth decrease with larger aperture. The increase results from usually the effect of seeing and observational circumstance, while the nonsteady dust emission and possibly the fading or destruction of dust grain bring the decrease (Lara et al. 2003; Tozzi et al. 2003).

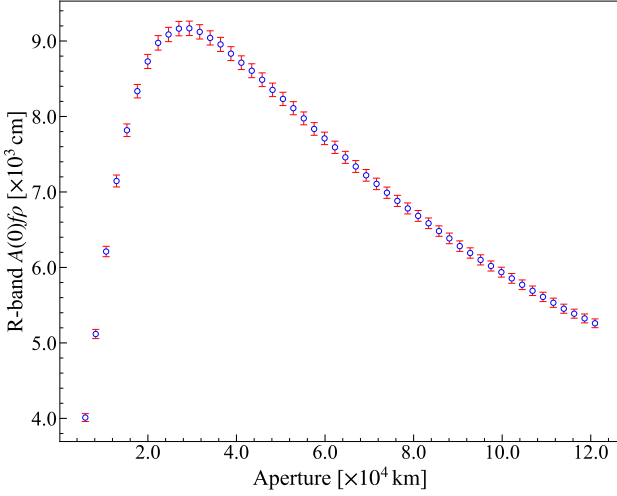
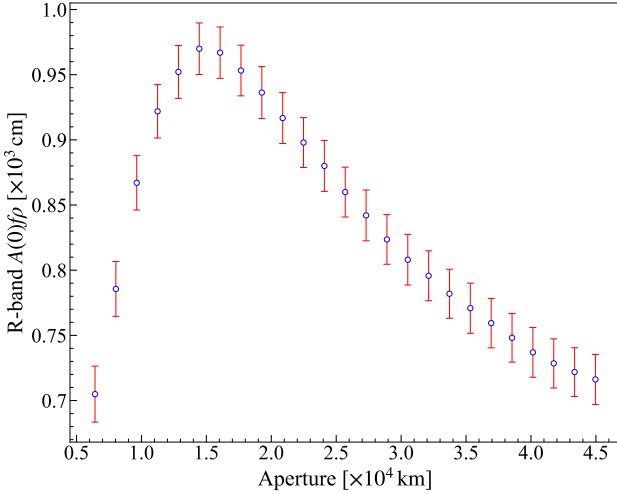
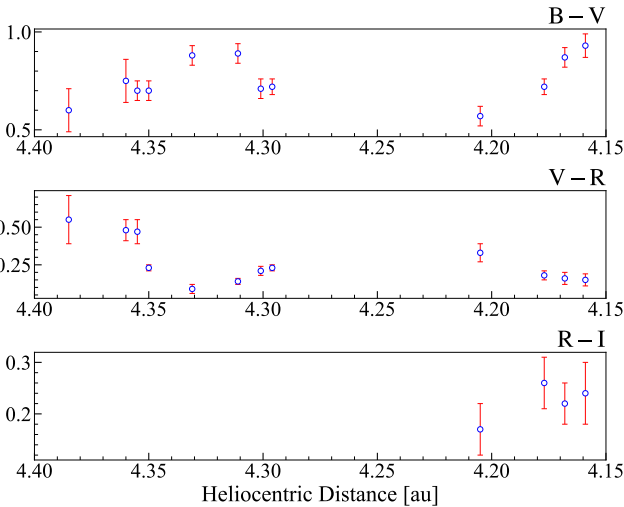
### 3.4 Coma Colors

The photometric results in Table 4 also summarises the color index of the two comets. Fig. 7 is the color indices  $B - V$ ,  $V - R$ , and  $R - I$  of C/2019 L3 as a function of heliocentric distance in au, all exhibiting variability during the approach to perihelion. As C/2019 L3 approached perihelion, its  $V - R$  color index showed a tendency towards blue. Considering its position at a heliocentric distance of about 4 au, with a temperature of around 140 K, the gas-driven effects are significant. The average colors for C/2019 L3 are as follows:  $\langle B - V \rangle = 0.75 \pm 0.06$ ,  $\langle V - R \rangle = 0.27 \pm 0.05$ , and  $\langle R - I \rangle = 0.22 \pm 0.05$ . On the other hand Besides, the colors for C/2020 P3 are  $B - V = 0.95 \pm 0.07$ ,  $\langle V - R \rangle = 0.29 \pm 0.05$ , and  $R - I = 0.21 \pm 0.05$ .

Moreover, in order to indicate how the scattered color of the dusty

<sup>8</sup> <https://asteroid.lowell.edu/comet/dustphase.html>

<sup>9</sup> [https://asteroid.lowell.edu/comet/dustphaseHM\\_table.html](https://asteroid.lowell.edu/comet/dustphaseHM_table.html)

(a) R-band  $A(0)f\rho$  of comet C/2019 L3 on 2021 May 14(b) R-band  $A(0)f\rho$  of comet C/2020 P3 on 2021 April 2**Figure 6.** R-band  $A(0)f\rho$  of comet C/2019 L3 and C/2020 P3.**Figure 7.** Color indices vs. heliocentric distance for C/2019 L3**Table 6.** Reddening of comet C/2019 L3 and C/2020 P3 with  $\rho = 2 \times 10^4$  km

Observation Time	B-band $Af\rho$	R-band $Af\rho$	reddening [%/kÅ]
<b>C/2019 L3</b>			
2021-03-28.729	9472 ± 753	12 811 ± 1764	13.75 ± 1.07
2021-04-02.739	8763 ± 806	10 719 ± 617	9.21 ± 0.50
2021-04-03.719	9886 ± 274	9538 ± 156	-1.65 ± 0.03
2021-04-04.691	9501 ± 343	8734 ± 93	-3.86 ± 0.07
2021-04-08.691	9288 ± 402	10 797 ± 725	6.89 ± 0.27
2021-04-12.724	12 683 ± 602	8979 ± 113	-15.69 ± 0.37
2021-04-14.702	8809 ± 382	8700 ± 110	-0.57 ± 0.01
2021-04-15.714	6077 ± 283	7173 ± 271	7.59 ± 0.23
2021-05-04.736	7724 ± 264	8065 ± 130	1.98 ± 0.04
2021-05-10.735	9030 ± 285	8891 ± 154	-0.71 ± 0.01
2021-05-12.724	9044 ± 336	7958 ± 326	-5.86 ± 0.16
2021-05-14.721	8428 ± 258	8475 ± 199	0.25 ± 0.01
<b>C/2020 P3</b>			
2021-05-12.749	934 ± 74	799 ± 37	-6.65 ± 0.01

coma varies with wavelengths, the reddening  $\mathcal{R}$  (or normalized color) (Jewitt & Meech 1986; Lara et al. 2003; Mazzotta Epifani & Palumbo 2011; Shi & Ma 2015) is calculated in units of [%/kÅ], with the formula given as equation (4):

$$\mathcal{R} = \frac{2}{Af\rho_1 + Af\rho_2} \frac{Af\rho_2 - Af\rho_1}{\lambda_2 - \lambda_1}, \quad (4)$$

where  $\lambda_1$  and  $\lambda_2$  are the central wavelengths of the filters in nm (respectively the centers of B and R filters, 440 nm and 658 nm). With this parameter it is convenient to indicate the percentage of change in the strength of the continuum per 1000 Å. The results of dust reddening are summarised in Table 6. In order to avoid the possible effects from background residuals, it is calculated with aperture of  $2 \times 10^4$  km.

For comet C/2019 L3, the reddening undergoes significant variations over time, from positive value ( $13.75 \pm 1.07$ ) [%/kÅ] on 2021 March 28 to negative value ( $-15.69 \pm 0.37$ ) [%/kÅ] on 2021 April 12. We plot the reddening as a function of date in Fig. 8, and the averaged value ( $0.94 \pm 0.23$ ) [%/kÅ] is marked as a horizontal blue dotted line. For comet C/2020 P3, only on 2021 May 12 is its observational data sufficient for the calculation of reddening with a result of ( $-6.65 \pm 0.01$ ) [%/kÅ].

The reddening of C/2019 L3 on each observation date is shown in Fig. 8, with the blue dotted line indicating the mean value. The plot reveals that over the observation course of nearly two months, C/2019 L3 exhibited multiple transitions from a reddish to a bluish color, possibly due to variations in the composition of the coma (Ivanova et al. 2017).

#### 4 DISCUSSION AND CONCLUSION

Comparing  $A(0)f\rho$  values with that of other LPCs, just as Fig. 9 shown, C/2019 L3 is very active at heliocentric distance of  $\sim 4$  au, and C/2020 P3 is moderately active at heliocentric distance of  $\sim 7$  au. Moreover, it can be seen from Fig. 10 that during the observation period, the R-band  $A(0)f\rho$  values of comet C/2019 L3, measured at an aperture of  $10^4$  km, showed a trend of initially decreasing followed by an increase. This could be attributed to a previous outburst, followed by a gradual increase in activity as it approaches perihelion. On the other hand, the BC-band  $A(0)f\rho$  value of C/2019 L3 up to  $(24 710 \pm 125)$  cm on 2022 January 19 posted on The As-

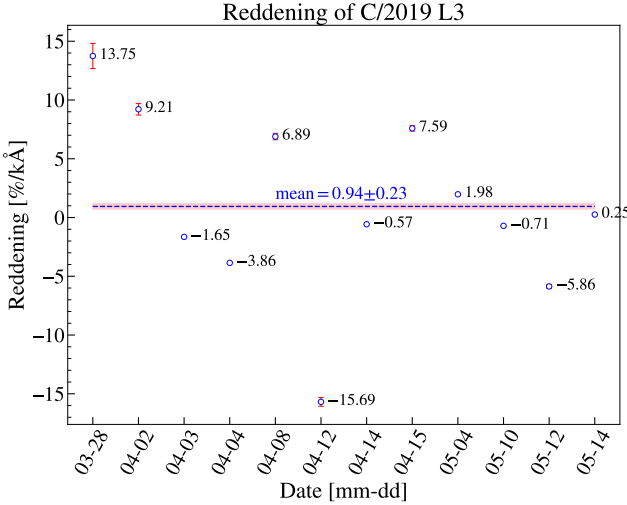


**Figure 8.** The reddening of comet C/2019 L3 with date, blue dashed line is the averaged reddening, and the surrounding red shadow shows the error.

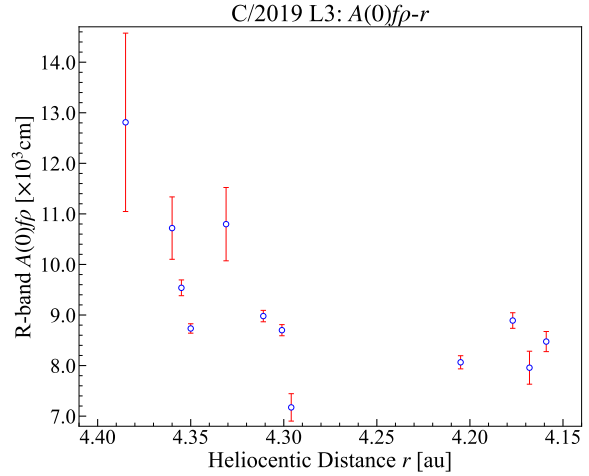


**Figure 10.** R-band  $A(0)f\rho$  values of C/2019 L3 as a function of heliocentric distance.

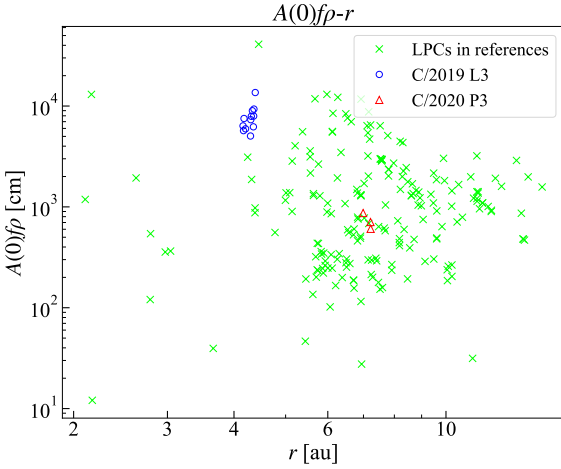


**Figure 9.**  $A(0)f\rho$  values measured in this work compared with that of other LPCs in literature by Mazzotta Epifani et al. (2014), Garcia & Gil-Hutton (2021), Garcia et al. (2020), Rousselot et al. (2014), Meech et al. (2009), Sárneczky et al. (2016), Solontoi et al. (2012), and Szabó et al. (2002). All data have been adjusted to phase angle  $0^\circ$ .

tronomer's Telegram<sup>10</sup>, with heliocentric distance  $r = 3.56$  au and geocentric distance  $\Delta = 2.61$  au, indicates that C/2019 L3 appears very active near the perihelion.

According to the study by Ramirez et al. (2012), the solar colors are as follows:  $(B - V)_\odot = 0.653 \pm 0.005$ ,  $(V - R)_\odot = 0.352 \pm 0.007$ , and  $(R - I)_\odot = 0.350 \pm 0.009$ . The average color indices of two Long-period comets and three dynamically new comets were calculated by Meech et al. (2009) to be  $\langle B - V \rangle = 0.76 \pm 0.01$  and  $\langle V - R \rangle = 0.43 \pm 0.01$ , with their heliocentric distances ranging from 5.8 au to 14.0 au. Solontoi et al. (2012) studied six Long-period comets within 5 au of the Sun and obtained the average color indices of  $\langle B - V \rangle = 0.687 \pm 0.005$  and  $\langle V - R \rangle = 0.443 \pm 0.003$ . Jewitt (2015) investigated Long-period comets with large range of heliocentric

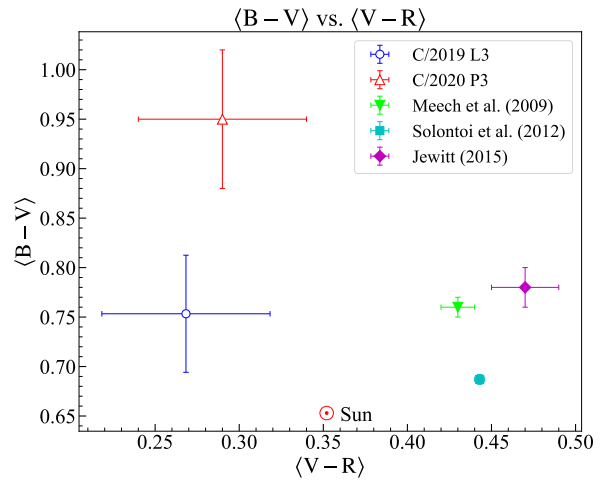


**Figure 11.** Color indices  $\langle B - V \rangle$  versus  $\langle V - R \rangle$  plot of Long-period comets

distances (1.875 au to 17.982 au), and the average color indices were found to be  $\langle B - V \rangle = 0.78 \pm 0.02$ ,  $\langle V - R \rangle = 0.47 \pm 0.02$ , and  $\langle R - I \rangle = 0.42 \pm 0.03$ .

Fig. 11 is the  $\langle B - V \rangle$  versus  $\langle V - R \rangle$  plot of C/2019 L3, C/2020 P3 and other LPCs. The color index of the Sun (Ramirez et al. 2012) is marked as a red circle with dot. As we can see, the  $\langle B - V \rangle$  colors of two comets are redder than the Sun, while the  $\langle V - R \rangle$  colors of them are bluer than the Sun. Compared with LPCs in other works, the  $\langle B - V \rangle$  color of C/2019 L3 is consistent with them, while the  $\langle V - R \rangle$  color of C/2019 L3 is significantly bluer than them. For C/2020 P3, the  $\langle B - V \rangle$  color is redder while the  $\langle V - R \rangle$  color is bluer. In general, the color indices of the two LPCs studied in this work differ from those of other LPCs.

In summary, we present the observational results of comets C/2019 L3 and C/2020 P3. The conclusions are as follows:

- (i) For comet C/2019 L3, A fan-shape structure can be observed in the northeast direction. This feature is visible in both V and R filters.

<sup>10</sup> <https://www.astronomerstelegram.org/?read=15186>

- (ii) The average gradient value of the surface brightness profile of comet C/2019 L3 is  $-1.66$ , suggesting a nonsteady coma.
- (iii) The R-band  $A(0)f\rho$  values of C/2019 L3 range from  $(5043 \pm 244)$  cm to  $(13\,611 \pm 1874)$  cm, and those of C/2020 P3 range from  $(606 \pm 31)$  cm to  $(869 \pm 20)$  cm. Compared to other works, the  $A(0)f\rho$  of C/2019 L3 is relatively high at  $\sim 4$  au, while that of C/2020 P3 is moderate at  $\sim 7$  au. The R-band  $A(0)f\rho$  values of C/2019 L3 tend to decrease first and then increase, so it is possible that comet C/2019 L3 experienced an outburst event in the past, and it was still active after this stage.
- (iv) The average colors for C/2019 L3 are  $\langle B - V \rangle = 0.75 \pm 0.06$ ,  $\langle V - R \rangle = 0.27 \pm 0.05$ , and  $\langle R - I \rangle = 0.22 \pm 0.05$ , while the colors for C/2020 P3 are  $B - V = 0.95 \pm 0.07$ ,  $\langle V - R \rangle = 0.29 \pm 0.05$ , and  $R - I = 0.21 \pm 0.05$ . The  $B - V$  colors of C/2019 L3 and C/2020 P3 are redder than the Sun, while the  $V - R$  and  $R - I$  colors of them are bluer than the Sun. Compared to other Long-period comets, both C/2019 L3 and C/2020 P3 exhibit distinct differences in their color indices. The reddening of C/2019 L3 calculated from B-band  $Af\rho$  and R-band  $Af\rho$  exhibits variations during the observational runs, from  $(13.75 \pm 1.07) \text{ \% / k\AA}$  to  $(-15.69 \pm 0.37) \text{ \% / k\AA}$  with an average value of  $(0.94 \pm 0.23) \text{ \% / k\AA}$ . This could be attributed to variations in the composition of the coma. As for C/2020 P3, the reddening could only be calculated for the date of 2021 May 12, yielding a value of  $(-6.65 \pm 0.01) \text{ \% / k\AA}$ .

## ACKNOWLEDGEMENTS

We thank the anonymous referee for the comments that improved the paper. We acknowledge the support of the B-type Strategic Priority Program of CAS (grant No. XDB41010104), the National Natural Science Foundation of China (Grant Nos. 12173093, 12033010) and the Natural Science Foundation of Jiangsu Province (BK20191512), the science research grants from the China Manned Space Project with No. CMS-CSST-2021-B08, the Space debris and NEO research project (Nos. KJSP2020020303, KJSP20200204, KJSP2020020102). We acknowledge the support of the Minor Planet Foundation of Purple Mountain Observatory.

## DATA AVAILABILITY

The data used in the paper is available from three different telescopes belonging to the International Scientific Optical Network (ISON) between 2021 March and 2021 May, namely the 1.0 m Zeiss-1000 telescope at Simeiz Observatory (Simeiz), the 2.6 m Shajn Telescope (ZTSh) at Crimean Astrophysical Observatory (CrAO), and the 0.7 m Maksutov meniscus telescope at Abastumani Astrophysical Observatory (AbAO). Data will be made available on request.

## REFERENCES

- A'Hearn M. F., Schleicher D. G., 1984, *AJ*, 89, 579
- Alexander C. M. O., McKeegan K. D., Altwegg K., 2018, *SSRv*, 214, 36
- Bauer J. M., Fernández Y. R., Protopapa S., Woodney L. M., 2022, Comet Science With Ground Based and Space Based Surveys in the New Millennium, <http://arxiv.org/abs/2210.09400>
- Betzler A. S., Diepvens A., de Sousa O. F., 2023, *MNRAS*, 526, 246
- Capria M. T., Coradini A., de Sanctis M. C., 2002, *EM&P*, 90, 217
- Fouchard M., Higuchi A., Ito T., 2023, *A&A*, 676, A104
- Garcia R., Gil-Hutton R., 2021, *P&SS*, 206, 105308
- Garcia R., Gil-Hutton R., García-Migani E., 2020, *P&SS*, 180, 104779
- Ivanova O., et al., 2017, *MNRAS*, 469, 2695
- Jewitt D., 2015, *AJ*, 150, 201
- Jewitt D., Meech K. J., 1986, *ApJ*, 310, 937
- Jewitt D. C., Meech K. J., 1987, *ApJ*, 317, 992
- Jewitt D., Agarwal J., Hui M.-T., Li J., Mutchler M., Weaver H., 2019, *AJ*, 157, 65
- Lara L. M., Licandro J., Oscoz A., 2003, *A&A*, 404, 373
- Lowry S. C., Fitzsimmons A., Cartwright I. M., Williams I. P., 1999, *A&A*, 349, 649
- Marcus J. N., 2007, *ICQ*, 29, 39
- Mazzotta Epifani E., Palumbo P., 2011, *A&A*, 525, A62
- Mazzotta Epifani E., Palumbo P., Capria M. T., Cremonese G., Fulle M., Colangeli L., 2009, *A&A*, 502, 355
- Mazzotta Epifani E., et al., 2014, *A&A*, 561, A6
- Meech K., et al., 2009, *Icar*, 201, 719
- Ootsubo T., et al., 2012, *ApJ*, 752, 15
- Prialnik D., 1992, *ApJ*, 388, 196
- Ramirez I., et al., 2012, *ApJ*, 752, 5
- Rousselot P., Korsun P. P., Kulyk I. V., Afanasiev V. L., Ivanova O. V., Sergeev A. V., Velichko S. F., 2014, *A&A*, 571, A73
- Samarasinha N. H., Larson S. M., 2014, *Icar*, 239, 168
- Samus' N. N., Kazarovets E. V., Durlevich O. V., Kireeva N. N., Pastukhova E. N., 2017, *ARep*, 61, 80
- Schleicher D. G., Bair A. N., 2011, *AJ*, 141, 177
- Shi J. C., Ma Y. H., 2015, *MNRAS*, 454, 3635
- Solontoi M., et al., 2012, *Icar*, 218, 571
- Szabó G. M., Kiss L. L., Sárneczky K., Sziládi K., 2002, *A&A*, 384, 702
- Sárneczky K., et al., 2016, *AJ*, 152, 220
- Tozzi G. P., Boehnhardt H., Lo Curto G., 2003, *A&A*, 398, L41
- Willmer C. N. A., 2018, *ApJS*, 236, 47
- Zacharias N., Finch C. T., Girard T. M., Henden A., Bartlett J. L., Monet D. G., Zacharias M. I., 2013, *AJ*, 145, 44
- Zacharias N., Finch C., Frouard J., 2017, *AJ*, 153, 166

This paper has been typeset from a  $\text{\TeX}/\text{\LaTeX}$  file prepared by the author.